Rough-wall boundary layers in adverse pressure gradients

By A. E. PERRY AND P. N. JOUBERT
Department of Mechanical Engineering, University of Melbourne

(Received 1 January 1963 and in revised form 22 April 1963)

Smooth- and rough-wall boundary layers and fully developed pipe and duct flow investigations are reviewed. It is shown that the effect of roughness on the flow away from the wall can be accounted for by using an equivalent viscosity ν_e. This viscosity is thought to depend only on the variables at the wall, such as shear stress τ_0, fluid density ρ, viscosity μ and the roughness size and geometry and that the relationship between these variables is the same for both boundary layers and duct flow. However, experiments to date have been confined to the 'rough régime' and to boundary layers with a zero pressure gradient.

Experiments were performed and the results show that the above finding can be extended to boundary layers with adverse pressure gradients in the rough régime.

A general method for measuring the local boundary-layer characteristics, with roughness and pressure gradients present, is developed.

1. Introduction

The effect of roughness on the development of turbulent boundary layers and the correlation of the results with the roughness effects in turbulent pipe flow is not only a subject of fundamental importance in fluid mechanics, but is also of importance in practical fields such as naval architecture and aeronautics. The correlation enables the more easily obtainable data of pipe flow to be applied to the outside surfaces of bodies having a similar roughness geometry as on the pipe surface. However, unlike smooth-wall flow investigations, the number of different conditions under which rough-wall flow have been examined to date is limited. As a result, smooth-wall data have often been used as a guide to predict how rough-wall flow might behave under the same conditions.

Many methods of calculation and analysis of the turbulent shear flow of a fluid near a wall hinge on the supposed existence of a logarithmic distribution of mean velocity U over some range of y from the wall. The fact that such a distribution exists has been verified by a large amount of experimental data for a variety of flow conditions and many models for the turbulence mechanism have been put forward to yield such a mathematical solution. However, the logarithmic profile can be arrived at by dimensional reasoning based on some simple experimental facts.

For fully developed flow in a uniform pipe of radius δ and with fluid velocity U_1 at the axis, a similarity defect law $(U_1 - U)/U_\tau = F(y/\delta)$ is found to exist except

in a thin layer adjoining the wall ($U_\tau = (\tau_0/\rho)^{\frac{1}{2}}$ where τ_0 is the wall shear stress and ρ the fluid density). A law of this form is also found to apply in zero-pressure-gradient boundary layers (where in this case δ is the boundary-layer thickness and U_1 is the free-stream velocity), although it is difficult to find a theoretical reason why such a law should hold exactly (see, for example, Rotta 1962).

Close to the wall in both boundary layers and pipes Prandtl's law of the wall is found to apply, i.e. $U/U_\tau = f(yU_\tau/\nu)$ even in the region of y where the defect law is applicable. Millikan (1939) pointed out that in the region of simultaneous validity of these two laws, the form of the function $f(yU_\tau/\nu)$ is mathematically restricted and is given by

$$\frac{U}{U_\tau} = \frac{1}{\kappa}\ln\frac{yU_\tau}{\nu} + A, \tag{1}$$

where κ and A are universal constants.

With pressure gradients imposed on a boundary layer, a similarity defect law does not exist although the law of the wall may still be applicable, as the experimental results of Ludwig & Tillman (1949) and the work of Clauser (1954, 1956) show. However, the defect law in pipes may be interpreted to mean that for a given 'shear velocity' U_τ, the effect of viscosity on the shape of the mean-flow profile is confined only to a thin layer adjoining the wall and this should also be true in boundary layers with and without pressure gradients. This information, when used in conjunction with the law of the wall, shows that a logarithmic profile should also occur in boundary layers without having to rely on a similarity defect law for the mathematical argument. This is shown by a modified form of Millikan's argument given by Rotta (1962).

From the law of the wall, the velocity gradient is given by

$$\frac{\partial U}{\partial y} = \frac{U_\tau^2}{\nu}\frac{df(yU_\tau/\nu)}{d(yU_\tau/\nu)},$$

and since this cannot depend on ν above the viscous sublayer, then

$$\frac{df(yU_\tau/\nu)}{d(yU_\tau/\nu)} = \frac{1}{\kappa}\left(\frac{yU_\tau}{\nu}\right)^{-1}, \tag{2}$$

where again κ is a universal constant. Integration then leads to equation (1). This equation is found to apply for approximately 15 % of the boundary-layer thickness. There appears to be a slight difference between the respective values of κ and A for the two situations of pipes and boundary layers quoted by various authors. However, in view of the scatter in results this possible difference is usually ignored.

One of the many significant results found by Nikuradse (1933) from his experiments on flow in pipes with sand-grain roughness was that the 'smooth wall' velocity defect law was still applicable irrespective of the size of the roughness. The effect of roughness on the velocity profile shape therefore is, like viscosity, confined to a thin region adjoining the surface and as far as the flow beyond this zone is concerned, roughness effects can be accounted for by using a modified coefficient of viscosity ν_e.

There will still exist a region where outside flow conditions given by δ and U_1 have no influence and, using the same arguments as used to arrive at equation (2) (with ν replaced by ν_e), a more general logarithmic law of the wall is obtained, namely

$$\frac{U}{U_\tau} = \frac{1}{\kappa}\ln\frac{yU_\tau}{\nu_e} + A. \tag{3}$$

Here κ is the same as for smooth surfaces and so also is the constant A by definition of ν_e.

2. Variables involved in rough-wall flow

Nikuradse's pipe data shows that ν_e depends only on the surface variables, which, for a given roughness geometry, are U_τ, ν and k where k is any length variable associated with the roughness size. Dimensional reasoning then leads to

$$\nu_e/\nu = f_1(kU_\tau/\nu) \tag{4}$$

and so equation (3) may be written in two other forms, these being

$$\frac{U}{U_\tau} = \frac{1}{\kappa}\ln\frac{y}{k} + B\left(\frac{kU_\tau}{\nu}\right) \tag{5}$$

or

$$\frac{U}{U_\tau} = \frac{1}{\kappa}\ln\frac{yU_\tau}{\nu} + A - \frac{\Delta U}{U_\tau}\left(\frac{kU_\tau}{\nu}\right). \tag{6}$$

Equation (5) is the form adopted by Nikuradse while equation (6) was the form used by Clauser (1954, 1956) and Hama (1954). When plotted on the basis of U/U_τ versus $\log(yU_\tau/\nu)$, equation (6) is represented by a family of straight parallel lines each being displaced downwards from the smooth wall profile by an amount $\Delta U/U_\tau$.

For low values of kU_τ/ν, ν_e is equal to ν, that is, roughness has no effect (the smooth régime). However, for high values of kU_τ/ν, viscosity plays no part (the rough régime) and equation (4) then gives

$$\nu_e = \alpha k U_\tau \quad \text{or} \quad \nu_e = k_e U_\tau,$$

where α is a constant dependent on the roughness geometry. The parameter k_e may be regarded as an effective roughness scale. Equation (3) becomes

$$\frac{U}{U_\tau} = \frac{1}{\kappa}\ln\frac{y}{k_e} + A, \tag{7}$$

and this is equivalent to equation (5) if B is a constant. The roughness function $\Delta U/U_\tau$ is given by

$$\frac{\Delta U}{U_\tau} = \frac{1}{\kappa}\ln\frac{k_e U_\tau}{\nu} + A. \tag{8}$$

It is suggested here that the parameter k_e is less arbitrary than the Nikuradse sand-grain scale which is now in wide-spread use. The parameter k_e is formed from a comparison with smooth surfaces and this would seem to be a more suitable standard.

For the intermediate values of kU_τ/ν where ν has an effect (the transition régime) the mathematical form of f_1 in equation (4) cannot be deduced by dimensional reasoning and the form will of course be different for different roughness geometries.

3. Review of rough-wall boundary-layer investigations

It has been assumed for many years that equations equivalent to (4) would be universally valid for both boundary-layer flow and fully developed pipe or channel flow for a given roughness geometry. For example, this was used as a basis in Schlichting's (1937) analysis for rough plates with zero pressure gradient or Prandtl & Schlichting's (1934) analysis. However, prior to 1951, little or no experimental work of worth had been carried out.

Moore (1951) obtained a useful set of experimental results for boundary layers with zero pressure gradient. His roughness consisted of square rods placed normal to the flow, the ratio of the pitch to height being 4; three sizes were used, these being $\frac{1}{8}$, $\frac{1}{2}$ and $1\frac{1}{2}$ in. squares. Unfortunately he attempted to verify the equations derived by Prandtl & Schlichting which were based on the distance x from the leading edge of the plate. The position of the effective leading edge is ill defined owing to lack of knowledge as to what happens where the boundary-layer thickness is comparable with the size of the roughness elements. Since the logarithmic law of the wall is applicable only for a distance of $y/\delta \simeq 0{\cdot}15$, it is possible that the roughness elements protrude into the layer for a distance much greater than this near the front of the plate.

Using expressions for skin friction based on a local length variable such as δ is also somewhat inaccurate unless it is defined on an integral basis as, for example, given by Coles (1956). From the similarity defect law and definition of the displacement thickness δ^*, Rotta (1950) arrived at another length variable Δ, given by

$$\Delta = \delta^* U_1/U_\tau = N\delta, \tag{9}$$

where N is a constant. Since Δ is proportional to δ and defined on an integral basis it would be an accurate substitute for δ in the skin-friction equation.

From an analysis of his boundary-layer profiles, Moore found that a similarity defect law was applicable and was identical with the smooth-wall law provided the origin for measuring y and δ was located some distance below the crest of the roughness elements.

With the more accurately defined variable Δ, Clauser (1954) arrived at the following law for skin friction with roughness effects included:

$$\sqrt{\frac{2}{c_f'}} = \frac{1}{\kappa}\ln(R_{\delta^*}) - \frac{\Delta U}{U_\tau} + D, \tag{10}$$

where $R_{\delta^*} = U_1\delta^*/\nu$. The variable D depends on the upstream shear and pressure distribution and is found to be approximately constant when the pressure gradient is zero. It is assumed that $\Delta U/U_\tau$ is not influenced by pressure gradients.

Clauser re-analysed the data of Moore on the basis of equation (10) and determined $\Delta U/U_\tau$ and found it to be an exclusive function of kU_τ/ν. This was compared with the flume data of Rand who used an identical roughness pattern and the same function was found to apply. Hama (1954) further confirmed the ideas of Clauser by carrying out zero-pressure-gradient boundary-layer tests with wire-screen roughness. The existence of a logarithmic law of the wall and a similarity defect law was strongly verified and the resulting $\Delta U/U_\tau$-variation

was compared with the flume data of Sarpkaya (see Hama 1954) and again this was found to be an exclusive function of kU_τ/ν.

The experimental data of Moore, Rand, Hama and Sarpkaya is shown in figure 1. It appears from this diagram that equation (4) is universally valid for a given roughness geometry since $\nu_e/\nu = \exp(\kappa \Delta U/U_\tau)$. However, the comparison between the flume and boundary-layer data was made only in the rough régime and for zero-pressure-gradient layers.

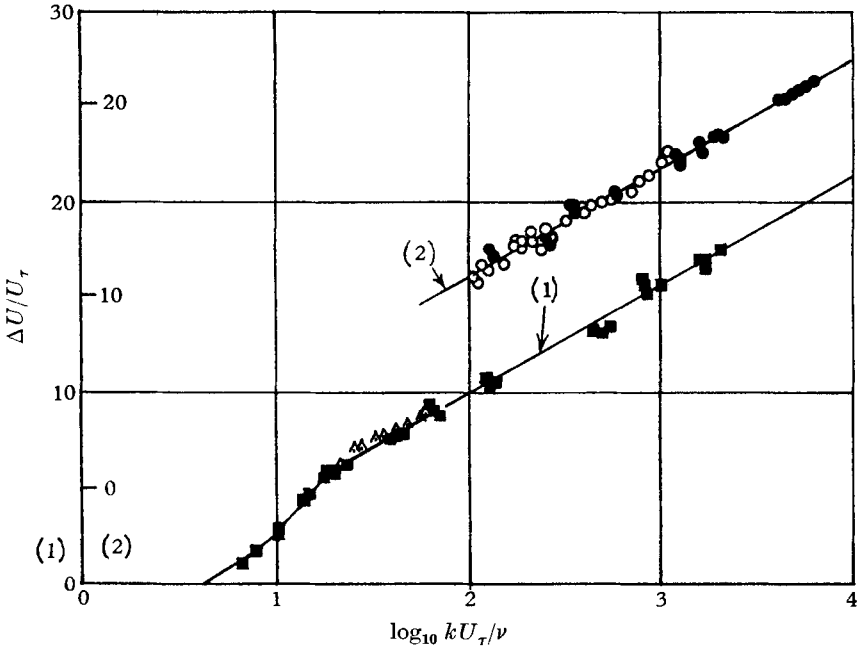

FIGURE 1. Roughness functions obtained from boundary layers and flumes. (1) Wire screens; (2) transverse bars. ■, Hama, boundary layer; △, Sarpkaya, flume; ●, Moore, boundary layer; ○, Rand, flume.

4. Aims

The aim of this work is to verify experimentally whether or not the above results would also be applicable to boundary layers with imposed arbitrary adverse pressure gradients. (Work is also progressing—not reported here—to establish laws for the above flow conditions for those roughness geometries which show a behaviour independent of roughness scale such as the 'groove'- and 'depression'-type roughness of Streeter & Chu 1949, Sams 1952 and Ambrose 1956.)

A further aim follows from difficulties associated with data reduction in this type of work. One reason why research on rough plates with pressure gradients has been avoided is that the various experimental techniques used for finding the local shear stress for smooth surfaces, such as the use of the Stanton or Preston tube or hot elements, cannot be applied unless the laws of roughness behaviour are known. Also momentum-integral methods with graphical differentiation are highly inaccurate, especially when pressure gradients are imposed. Pressure-

tapped roughness elements or floating-element techniques could be employed. However, the form of the roughness elements are restricted by this and so these methods are not always convenient. A more universal method of data reduction was thought to be of greater use.

5. Description of apparatus

5.1. *Wind tunnel*

The Melbourne University wind tunnel was used for the tests, it being of the closed circuit type with a contraction and diffusing working section of octagonal form. The contraction measured 5 ft. 6 in. wide by 4 ft. 3 in. high at its downstream end. A closed working section 17 ft. long was installed which matched the contraction and expanded along its length to a basic cross-section 6 ft. $1\frac{1}{2}$ in. wide by 5 ft. 3 in. high. A turbulence screen was erected in the settling section of the

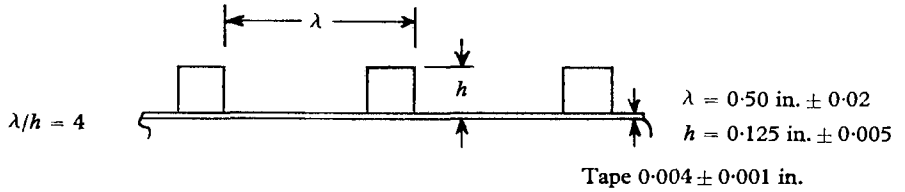

FIGURE 2. Roughness geometry tested.

tunnel which reduced the turbulence level from 1·0 to 0·56 % as measured by a 6 in. diameter turbulence sphere when the tunnel was empty and corresponded to 90 ft./sec. at the contraction exit. This was of some importance since Coles's wake function is sensitive to turbulence level when it is above approximately 0·5 % and the data reduction depended on an accurate wake.

5.2. *Plate*

The plate was made to fit horizontally across the tunnel and its width varied to suit the working section. It was provided with slotted brackets to allow for adjustment for the various desired pressure gradients. Felt seals were fitted between the plate edges and tunnel walls.

One panel of the plate extended 3 ft. into the contraction and a tailpiece extended 4 ft. into the diffuser and this gave a total length of plate equal to 24 ft. However, it was found necessary to traverse only 17 ft. of plate. A special nosepiece was fitted to the leading edge to allow for smooth entry of the flow when the plate was tilted for adverse pressure gradients.

5.3. *Roughness elements*

In order to correlate resistance and roughness-function measurements with pressure gradients imposed with those of other workers who used zero pressure gradients, the same roughness as used by Moore was chosen. The roughness geometry is shown in figure 2. A typical velocity profile will be referred to here as II 3 say. The Roman numeral refers to the pressure gradient imposed and the arabic number refers to the traverse number in the series.

The roughness consisted of 800 strips of timber which were accurately machined to size and were 5 ft. 3 in. in length. These were held to the plate by strips of double-coated adhesive tape.

Since at the downstream end, the roughness did not span the full width of the tunnel, it was felt that this may have introduced additional three-dimensional effects. However, it did not appear to affect the results.

6. Experimental procedure

All velocity traverses were carried out normal to the plate and along the tunnel centre-line. The distance y_T measured from the top of the elements to the centre-line of the probe had its origin located by means of an electrical contact method and could be reproduced within the limits of $\pm$ 0·001 in. and the value of y_T could be measured and controlled to this accuracy.

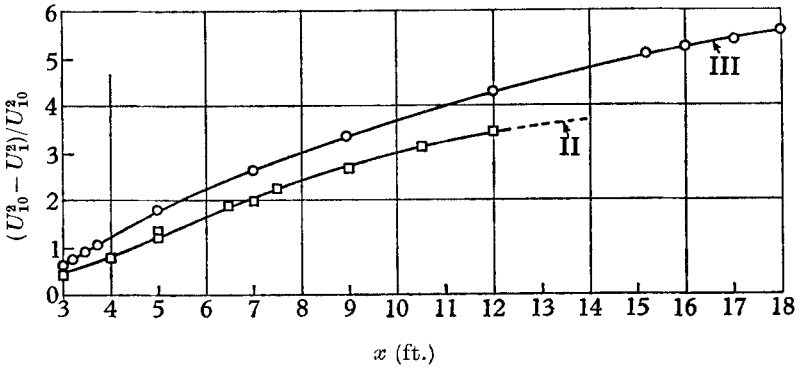

FIGURE 3. Pressure distributions II and III.

It was not clear at first to which position relative to an element the velocity profile should be measured. This position, however, was found to make no difference to the resulting profile. All pressure coefficients were based on the velocity U_{10} which was measured in the free stream 2 ft. 6 in. from the leading edge of the plate. The static pressure variation through the profile was also noted and was found to be negligible in all cases even for the profiles which were 13 in. thick. Hence the usual boundary-layer approximation could be used if found to be necessary.

The pressure distributions used (II and III) are shown in figure 3 and were obtained from velocity measurements.

7. Analysis of data reduction methods

7.1. *Basic principles of 'local profile' method*

A graphical method was developed for determining the local boundary-layer characteristics from each measured velocity distribution and this method is an extension of a method introduced by Clauser (1954) which is suitable for smooth surfaces with and without pressure gradients.

Using the usual law of the wall

$$\frac{U}{U_\tau} = \frac{1}{\kappa}\ln\frac{yU_\tau}{\nu} + A,$$

a multiplication of both sides by U_τ/U_1 ($= \frac{1}{2}c_f')^{\frac{1}{2}}$ leads to the form

$$\frac{U}{U_1} = 5{\cdot}6\sqrt{\frac{c_f'}{2}}\log_{10}\frac{yU_1}{\nu} + 5{\cdot}6\sqrt{\frac{c_f'}{2}}\left(\log_{10}\sqrt{\frac{c_f'}{2}} + 0{\cdot}875\right),$$

where here the numerical values $\kappa = 0{\cdot}41$ and $A = 4{\cdot}9$ are being used. These are the average values arrived at by Clauser from various sources.

It can be seen from the above equation that on a U/U_1 versus $\log_{10}(yU_1/\nu)$ plot, a family of straight lines is produced, each line corresponding to a given value of c_f'. Thus a chart may be constructed, and by plotting the experimental points on such a chart, the line upon which they fall gives the appropriate value of c_f'. The accuracy of the result is confirmed by two properties of the line, these being its slope and its placement on the chart.

It will be assumed for the moment that this method can be extended to rough surfaces. Here difficulties arise, these being that the origin for y is not known and also, since the roughness causes a shift in the logarithmic profile, the value of c_f' is confirmed only by the slope of the logarithmic line and not its position.

For the velocity U, let y_T be the distance above the crests of the elements and y be the distance from the logarithmic asymptote, this being located a distance ϵ below the crests. It will be further assumed that Coles's wake hypothesis is applicable (Coles 1956) so that the whole profile is described by

$$\frac{U}{U_\tau} = \frac{1}{\kappa}\ln\frac{yU_\tau}{\nu} + A - \frac{\Delta U}{U_\tau} + \frac{\Pi}{\kappa}\omega\left(\frac{y}{\delta}\right), \tag{11}$$

where ω is a supposed universal function of y/δ and Π is a parameter dependent on the upstream shear stress and pressure distribution.

From this it can be shown that

$$\frac{U}{U_1} = \frac{1}{\kappa}\sqrt{\frac{c_f'}{2}}\ln\left\{\frac{(y_\tau+\epsilon)\,U_1}{\nu}\right\} + \sqrt{\frac{c_f'}{2}}\left\{\frac{1}{\kappa}\ln\sqrt{\frac{c_f'}{2}} + A - \frac{\Delta U}{U_\tau}\right\} + \sqrt{\frac{c_f'}{2}}\frac{\Pi}{\kappa}\omega\left(\frac{y}{\delta}\right).$$

This can be put into the more experimentally convenient form using Clauser's numerical values

$$\frac{U}{U_1} = 5{\cdot}6\sqrt{\frac{c_f'}{2}}\log_{10}\{y_\tau+\epsilon\} + P + \frac{\Pi_0}{2}\omega\left(\frac{y}{\delta}\right), \tag{12}$$

where here y_T and ϵ are measured in inches if P is given by

$$P = \sqrt{\frac{c_f'}{2}}\left\{5{\cdot}6\log_{10}\frac{U_1}{\nu}\sqrt{\frac{c_f'}{2}} + 5{\cdot}6\log_{10}1\tfrac{1}{2} + 4{\cdot}9 - \frac{\Delta U}{U_\tau}\right\}. \tag{13}$$

From this $\Delta U/U_\tau$ is given by

$$\frac{\Delta U}{U_\tau} = 5{\cdot}6\log_{10}\frac{U_1}{\nu}\sqrt{\frac{c_f'}{2}} - \frac{P}{(\frac{1}{2}c_f')^{\frac{1}{2}}} - 1{\cdot}14. \tag{14}$$

Also

$$\Pi = \frac{\kappa\Pi_0}{2}\sqrt{\frac{2}{c_f'}} = 2{\cdot}05\Pi_0\sqrt{\frac{2}{c_f'}}. \tag{15}$$

Equation (12) is shown dotted in figure 4 and represents the experimental points that would be actually plotted during a traverse, it being a plot of U/U_1 versus $\log_{10} y_T$ (in.). Once the error ϵ is known, an addition of it to each y_T value would give the curve shown full in the figure. For low values of $\omega(y/\delta)$ this curve follows the asymptote XX for some considerable distance on the semi-logarithmic plot.

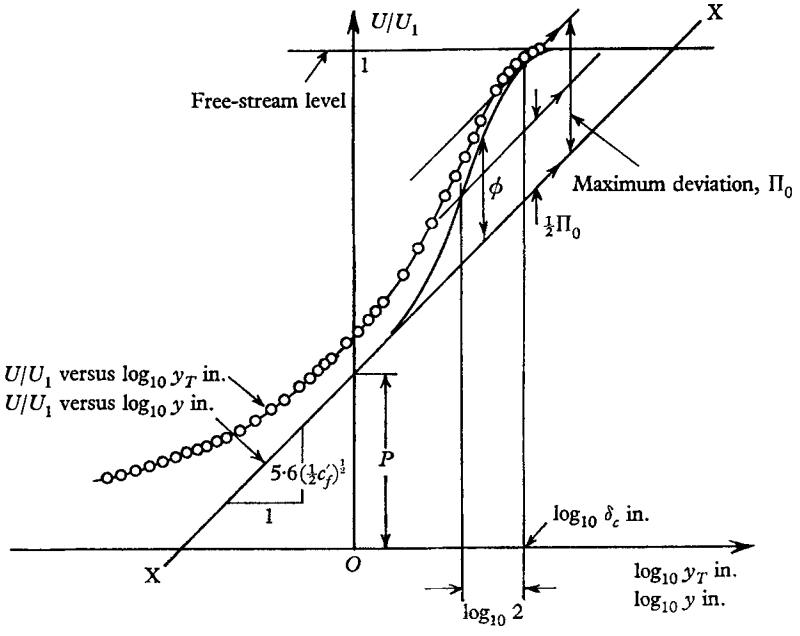

FIGURE 4. Graphical method for determining boundary-layer and roughness variables and functions.

From equation (12) the slope of XX gives the value of $5{\cdot}6(\frac{1}{2}c_f')^{\frac{1}{2}}$ while the vertical intercept gives P. From this

$$\frac{hU_\tau}{\nu}\left(=\frac{hU_1}{\nu}\sqrt{\frac{c_f'}{2}}\right)$$

can be calculated and knowing P a simple calculation using equation (14) gives the value of $\Delta U/U_\tau$. Here h is the height of the roughness element.

The boundary-layer thickness δ may be found rapidly and with reasonable accuracy by using the properties of the wake function $\omega(y/\delta)$. Coles defined δ on an integral basis

$$\left(\omega(1) = z \quad \text{and} \quad \int_0^2 \left(\frac{y}{\delta}\right) d\omega = 1\right),$$

but also pointed out that if the wake function is to be universal, δ must also correspond to the value of y at which the maximum deviation from the logarithmic profile occurs. From equation (12) it can be seen that this maximum deviation will equal Π_0 (since $\omega(1) = 2$) and from equation (15) Π can be found. The point of maximum deviation is difficult to find since it occurs at a point of tangency. However, since the wake is nearly antisymmetrical, a line drawn

parallel to the asymptote XX and at half the maximum deviation away (a construction suggested by Coles) will cut the profile at half the boundary-layer thickness. Hence it can be seen from figure 4 that adding $\log_{10} 2$ to the value of $\log_{10} y$ at which this intersection occurs will give the boundary-layer thickness.

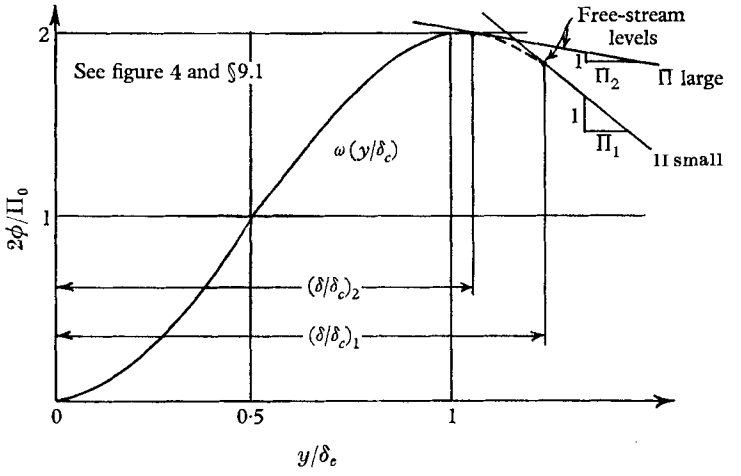

FIGURE 5. Relationship between Coles's thickness δ_c and δ.

Unfortunately the wake function is not truly universal at the outer edge of the layer since it asymptotes to a line of slope $-1/\Pi$ instead of zero, as shown in figure 5. This can be shown from equation (11) together with the condition that $(\partial U/\partial y)_{y=\delta} = 0$. Figure 5 also shows that the point of maximum deviation does not correspond to the true boundary-layer thickness δ but to a thickness which will be referred to as δ_c. When based on this, Coles's wake function becomes nearly universal. As Π becomes large δ_c will approach δ and for small Π it will be hoped (for the moment) that the discrepancy is not very large.

With some saving of effort, the above analysis could have been based on the roughness function B. However, to keep it in line with the analysis of Clauser and Hama $\Delta U/U_\tau$ was adopted.

7.2. *Approximate method for locating the origin of y*

For an accurate determination of c_f' and other parameters, an accurate estimate of ϵ is required and this proved to be one of the most difficult tasks in the present project. An error in origin for y distorts the logarithmic profile into a curve on the semi-logarithmic plot.

It can be shown that for a given slope of logarithmic line, a positive value of ϵ produces a curve with a horizontal asymptote which intersects the logarithmic line at $\ln y = \ln \epsilon$ and the shape of the curve is indepenent of ϵ (see figure 6). For negative values of ϵ, the asymptote is vertical and such curves are also shown. A chart based on this principle was constructed and enabled c_f' and ϵ to be determined, but it proved to be extremely insensitive since many combinations of ϵ and c_f' gave equally good fits to the experimental points.

After much experimenting, the writers found that the following method, although not giving the precise value of ϵ, locates the narrowest range within which it occurs. Adding an error, which is larger than say twice the expected

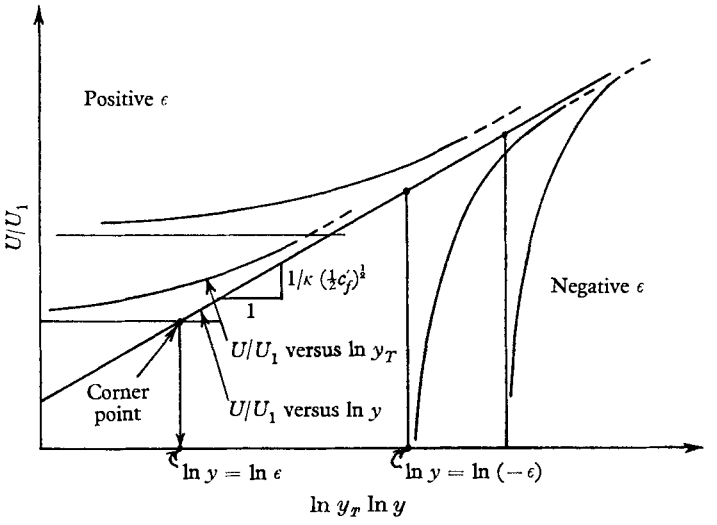

FIGURE 6. Figure showing curves of constant error, ϵ.

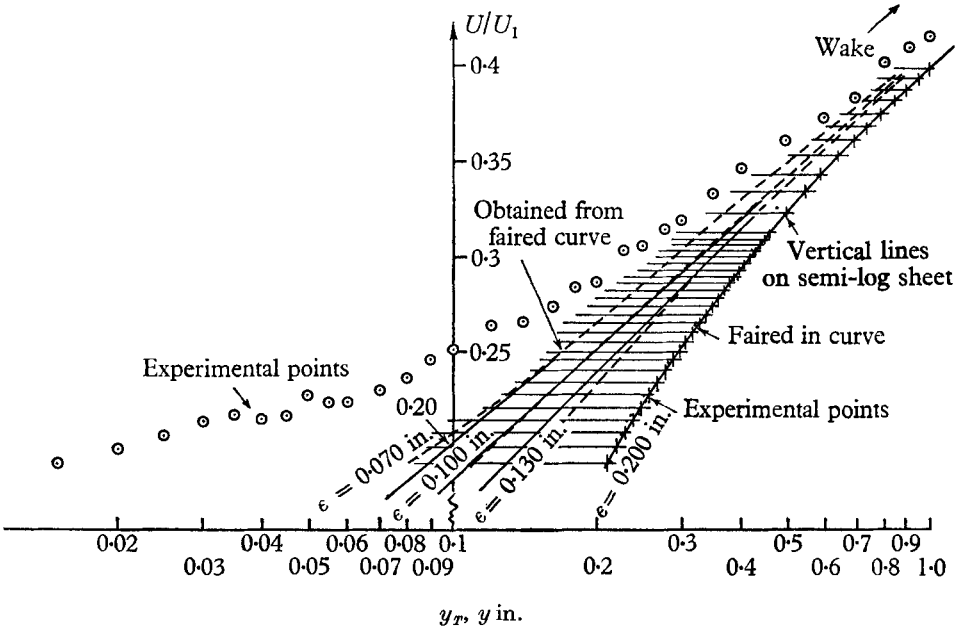

FIGURE 7. Graphical method for finding range of likely ϵ values.

value in the experimental plot, gives curves which have the trend corresponding to negative values of ϵ shown in figure 6. This brings the experimental points close together, making it very easy to 'eye-in' a monotonic curve of best fit. Points near the surface which may be off the logarithmic line show up clearly

and can be ignored while the region where the wake deviates shows up as a sharp inflexion. (This is not so for small values of Π.)

Using this faired-in curve, errors are then subtracted, giving a family of straight or nearly straight lines in the region of the true value of ϵ. (If actual experimental points are used instead of the faired-in curve, a conglomeration of scattered points is produced in this region.) A typical construction is shown in figure 7 from an actual experimental profile.

The wake component should deviate at y/δ equal to 0·1 to 0·15. This acts as a useful guide for finding the region of the profile which is logarithmic.

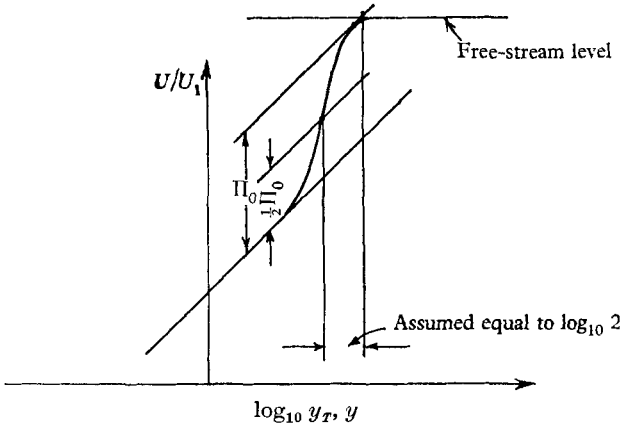

FIGURE 8. Wake alignment method for finding ϵ (Π large).

7.3. *'Wake alignment' method for finding ϵ precisely*

When Π is large, it was seen in § 7.1 that δ_c approaches δ and if the wake hypothesis is accepted, the correct value of ϵ may be found by extending the line tangent at the point of maximum deviation up to the free-steam level cutting this at a well-defined point as shown in figure 8. The distance between this point and the intersection at half the maximum deviation should approach $\log_{10} 2$ on the horizontal scale. By doing this for a few likely values of ϵ, an interpolation scheme can be used to give a fairly precise and consistent value of ϵ and hence c_f'.

7.4. *Checking of local profile method*

The above method relies on the existence of a logarithmic law and this is one of the facts to be proved. Also the value of κ used may not be applicable to rough surfaces, that is, roughness may affect the flow for some considerable distance from the wall. Hence an independent check is required for completeness.

The momentum integral equation may be written in the form

$$\frac{c_f'}{2} = \frac{\theta}{U_1}\{2+H\}\frac{dU_1}{dx} + \frac{d\theta}{dx}, \tag{16}$$

where θ is the momentum thickness and $H = \delta^*/\theta$. This equation is then integrated thus avoiding graphical differentiation,

$$\int_{x_1}^{x} \tfrac{1}{2}c_f' dx = \int_{U_{11}}^{U_1} \frac{\theta}{U_1}\{2+H\}dU_1 + \theta - \theta_1. \tag{17}$$

By integrating from the back of the plate, say at $x = x_1$, to a general value of x the difference being Δx, the right-hand side of equation (17) was plotted against Δx from measurements of the profile and the x-wise velocity distribution. The left-hand side was determined from the results of the wake-alignment method and plotted against Δx for comparison. This acted as a fairly accurate check (see § 9.1).

8. Discussion of data reduction

The wake-alignment method was used, and although the writers do not recommend this for values of Π less than unity, only the leading-edge profiles II 1* and II 2 showed any appreciable discrepancy with the resulting trend.

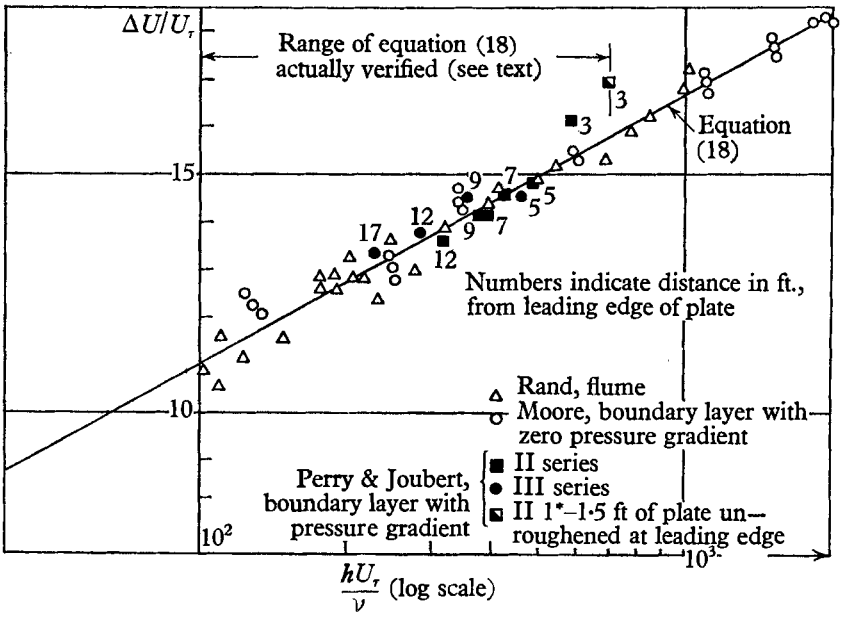

FIGURE 9. Roughness function.

Profile II 6 gave a contradictory result in the value of ϵ predicted by the logarithmic law and wake but this was found to be due to an ill-defined free-stream level. The free-stream velocity was not uniform at this section and so trial-and-error methods were used to give a symmetrical wake.

Profile III 1 failed to yield a solution since there was insufficient length of logarithmic region to confirm a definite slope.

9. Discussion of results

Figure 9 shows the resulting distribution of $\Delta U/U_\tau$ versus $\log_{10}(hU_\tau/\nu)$ and also shown are the results obtained by Rand (flume) and Moore (flat plate with zero pressure gradient) (see § 3). All pertinent data is shown in table 1. These latter results were scaled from a smaller diagram given by Hama (1954) and so the exact distribution is not guaranteed, although the amount of experimental scatter has been reproduced fairly closely The results obtained here appear to

agree fairly well for both pressure distributions and the accuracy of the method employed compares well with the more easily obtainable consistency from a flume or zero-pressure-gradient layer. The line drawn in this figure is the average of the Moore–Clauser and Rand results and its equation is given fairly closely by

$$\Delta U/U_\tau = 5{\cdot}6 \log_{10}(hU_\tau/\nu) - 0{\cdot}2. \tag{18}$$

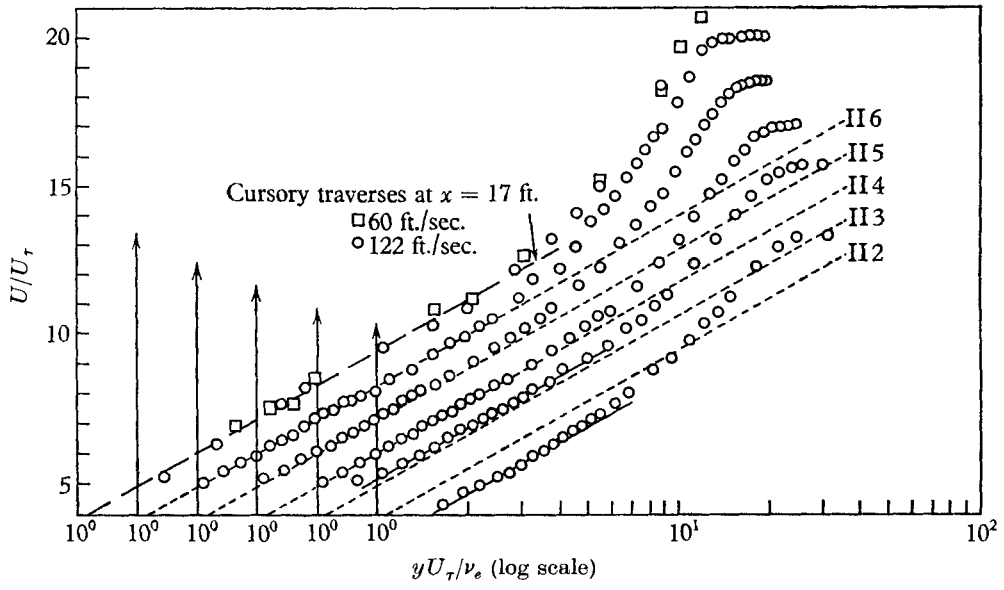

FIGURE 10. Experimental velocity profiles, II series. – – – –, Equation (3) deduced from mean line of Moore–Rand results (see text).

The measured velocity profiles were compared with the universal law of the wall $U/U_\tau = f(yU_\tau/\nu_e)$ as obtained from equation (18) and are shown in figures 10 and 11. All profiles have been displaced horizontally from each other to avoid confusion with the experimental points. It can be seen from these figures that the agreement is good and that the size of the wake has no influence on the logarithmic law of the wall. The figures also give an idea of the range of logarithmic profiles measured. (Every second point has been omitted below $y - \epsilon = 0{\cdot}06$ in.).

The wake components are compared with Coles's tentative wake function in figure 12, only the best and the worst results being shown.

9.1. *Checking of method*

Figure 13 shows for the III series the skin-friction coefficient c_f' as obtained by the wake-alignment method and the momentum-integral method using graphical differentiation. It can be seen that the results are considerably scattered. However, a comparison of the integrated momentum-integral equation with the integrated wake-alignment c_f'-distribution (as outlined in § 7.4) is shown in figure 14. These quantities were found by integrating upstream from the last downstream profile so that any errors made near the leading edge would not show up right through the calculation as an 'integration constant'. The agree-

ment shown in these figures is fair, the III series being more accurate because of the larger II values. A plot of the II values is shown in figure 15 for the two pressure distributions.

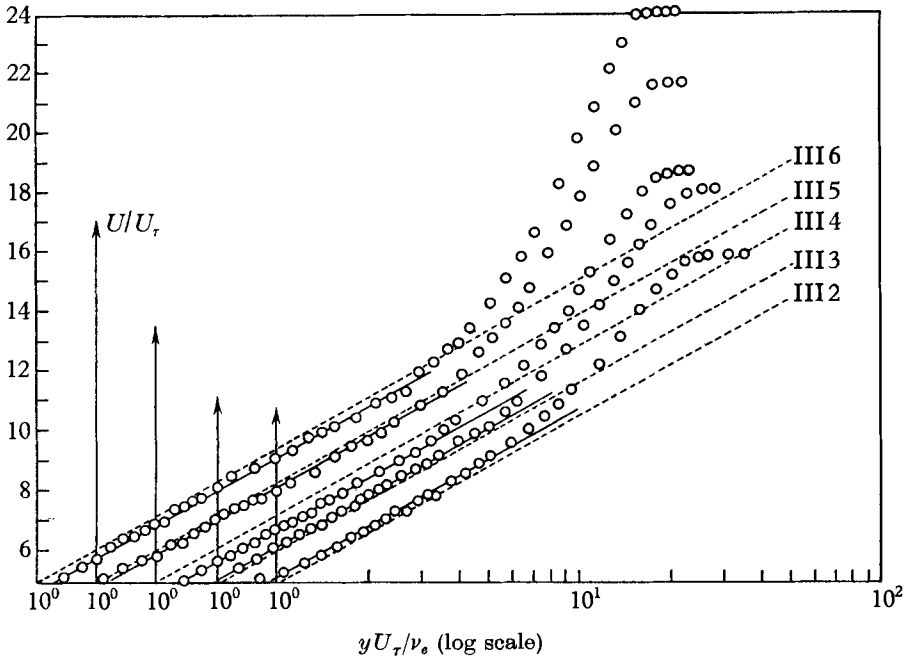

FIGURE 11. Experimental velocity profiles, III series. ——, Equation (3) deduced from mean line of Moore–Rand results (see text).

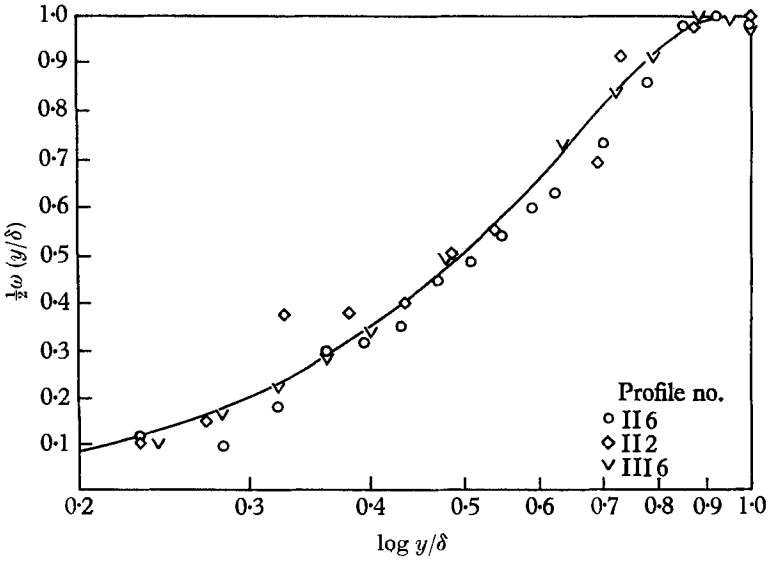

FIGURE 12. Comparison with Coles's wake function.

Profile no.	U_1 (ft./sec.)	x (ft.)	P	$5{\cdot}6(\frac{1}{2}c_f')^{\frac{1}{2}}$	Π_0	δ_c (in.)	ϵ (in.)	$\frac{hU_\tau}{\nu} \times 10^{-2}$	$\frac{\Delta U_\tau}{U}$
II 1†	119	3	0·784	0·49	0·126	1·53	0·085	6·95	16·9
2	119	3	0·706	0·22	0·182	1·86	0·100	5·94	16·1
3	113	5	0·662	0·36	0·18	2·72	0·080	4·84	14·74
4	109	7	0·60	0·33	0·20	4·0	0·100	4·26	14·56
5	104	9	0·555	0·303	0·23	5·15	0·100	3·77	14·11
6	99·4	12	0·506	0·280	0·253	6·6	0·100	3·21	13·5
III 1	118	3	—	—	—	—	—	—	—
2	110	5	0·653	0·351	0·18	2·56	0·080	4·62	14·46
3	105	7	0·570	0·308	0·228	4·35	0·115	3·86	14·11
4	100	9	0·523	0·299	0·252	5·7	0·120	3·55	14·46
5	92·6	12	0·462	0·229	0·305	8	0·100	2·86	13·66
6	83·6	17	0·407	0·259	0·34	12·6	0·100	2·29	13·34

† 1 ft. 6 in. of plate unroughened at leading edge.

TABLE 1. Experimental data.

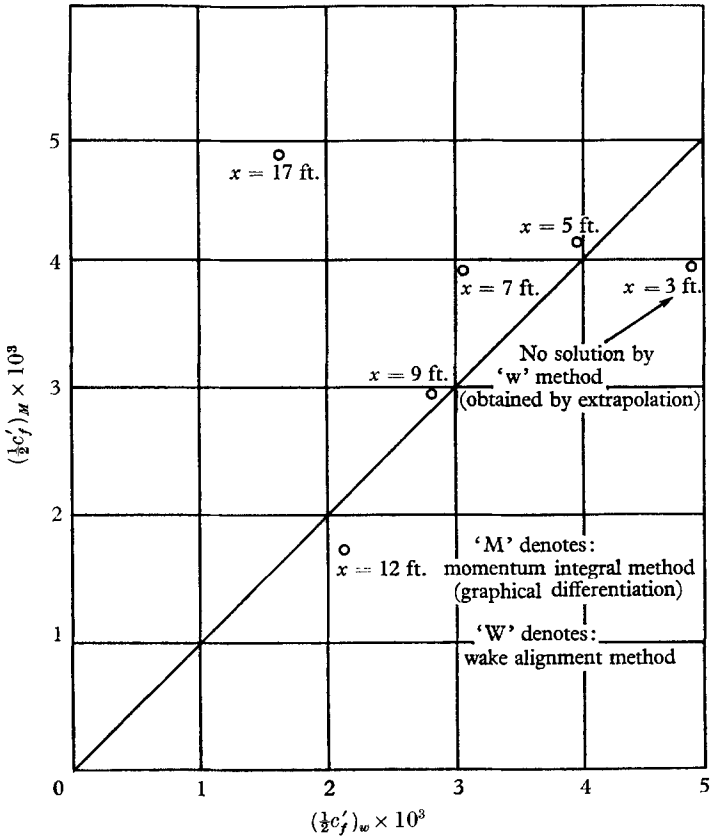

FIGURE 13. Comparison of methods, III series.

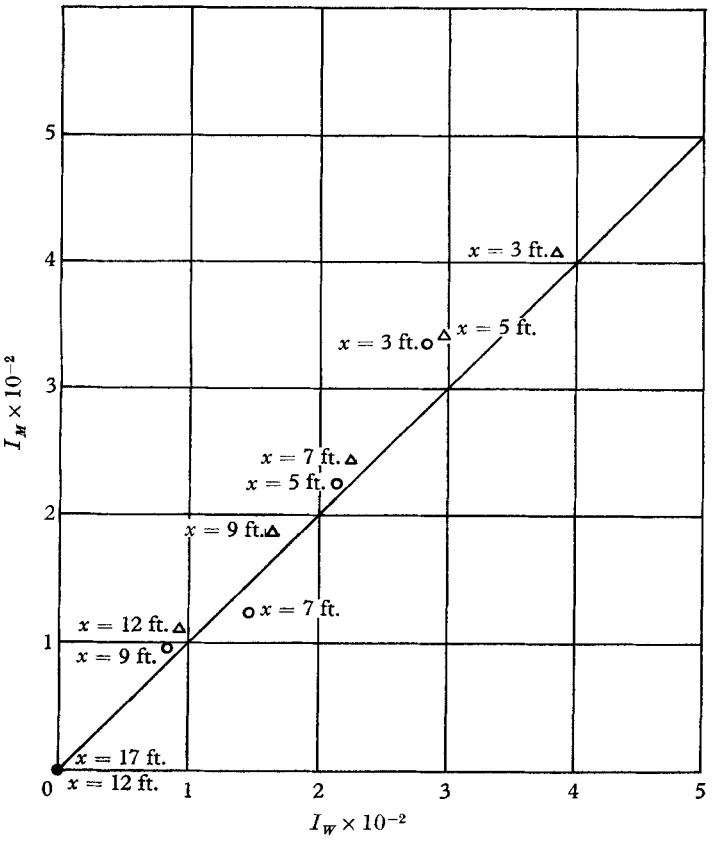

FIGURE 14. Checking of wake alignment method.

$$I_M = \int_{U_{11}}^{U_1} \frac{\theta}{U_1}\{2+H\}\,dU_1 + \theta_x - \theta_1, \quad I_W = \int_{x_1}^{x} \tfrac{1}{2}c_f'\,dx,$$

as obtained from wake alignment results. ○ Pressure distribution II; △, pressure distribution III.

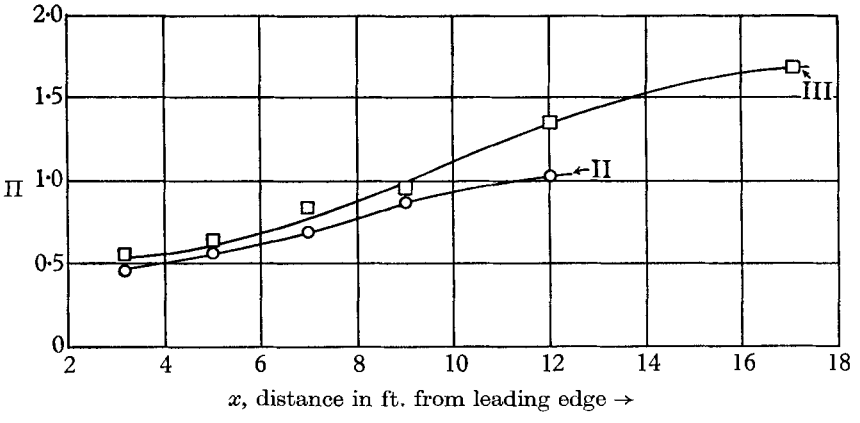

FIGURE 15. Coles's wake factor, II, for II and III series.

9.2. *Error in origin*

Table 1 shows that the error in origin ϵ was fairly constant, it being approximately 0·1 in. on the average. The total thickness of the measuring probe was approximately 0·030 in., this causing a small displacement in the effective distance from the wall. However, the correction to be made for this is negligible compared with the size of the roughness elements and the value of ϵ corresponds to 0·8 of the roughness height, this being only slightly different from the results of Moore. He estimated this value to be approximately 0·7.

9.3. *Value of viscosity adopted*

The results for these tests were not temperature corrected for viscosity ν since all flow was in the rough régime and ν entered only as a matter of definition for $\Delta U/U_\tau$. A variation in ν merely shifts the points given in figure 11, parallel to the mean line. The value of viscosity adopted was $\nu = 1{\cdot}56 \times 10^{-4}$ ft.^{2}/sec.

9.4. *Range of variation of parameters*

The results shown in figure 9 cover about three-quarters of a decade and this compares well with the range obtained by Moore who covered two decades (see figure 1). However, Moore used three sizes of roughness and a fairly large speed variation (30 to 80 ft./sec.), while here only one tunnel speed and one roughness size was used. This shows an advantage in using adverse pressure gradients. It is possible to control the speed of the tunnel so that the results would extend down another $\frac{2}{3}$ of a decade and perhaps reach into the transition régime. However, it is likely that hot-wire traverses would then be needed. The actual range over which the mean line shown in figure 9 was verified is indicated by the arrow heads. This was done by making two cursory traverses near the trailing edge of the plate at two different tunnel velocities (60 ft./sec. and 122 ft./sec. at the nozzle; $x = 17$ ft.; pressure distribution II). By noting on a U/U_1 versus $\log_{10} y_T$ plot a near identity of the two profiles it was concluded that viscosity did not enter the problem to any significant extent and so the flow was rough in this range. These two cursory traverses were normalized so that they could be plotted in figure 10 (ϵ was assumed to be 0·1 in. and a knowledge of U_τ was not necessary although it was known approximately).

10. Conclusions and recommendations

(i) The method employed for determining the various boundary-layer characteristics with roughness and pressure gradient effects included met with success when the parameter Π was large. For values of Π much less than unity (leading edge profiles), the method met only with moderate success.

(ii) For rough-régime flow, the roughness function was found to be independent of the pressure gradients imposed. Experiments should now be carried out with pressure gradients of sufficient strength to influence the logarithmic profile. However, pressure-tapped roughness elements will probably be required since the methods of data reduction used here depend on the existence of a reasonably large logarithmic region.

REFERENCES

AMBROSE, H. H. 1956 The effect of surface roughness on velocity distribution and boundary resistance. University of Tennessee, Department of Civil Engineering Contract N/r 811(03). Office of Naval Research Department of the Navy.

CLAUSER, F. H. 1954 Turbulent boundary layers in adverse pressure gradients. *J. Aero. Sci.* **21**, 91.

CLAUSER, F. H. 1956 The turbulent boundary layer. *Appl. Mech.* **4**, 1–51.

COLES, D. 1956 The law of the wake in the turbulent boundary layers. *J. Fluid Mech.* **1**, 191–226.

HAMA, F. R. 1954 Boundary layer characteristics for smooth and rough surfaces. *Trans. Soc. Naval Arch. Mar. Engrs*, **62**,

LUDWIG, H. & TILLMAN, W. 1949 Untersuchungen veber dis Wandschub in turbulenten Reibungsschichten. *Ing-Arch.* **17**, 288–99. Translated as 'Investigations of the wall shearing stress in turbulent boundary layers', *NACA TM*, no. 1285.

MILLIKAN, C. D. 1939 Turbulent flows in channels and circular tubes. *Proc. Fifth Int. Congr. Appl. Mechanisms*, pp. 386–92.

MOORE, W. F. 1951 An experimental investigation of the boundary layer development along a rough surface. Ph.D. dissertation, State University of Iowa.

NIKURADSE, J. 1933 Strömungsgesetze in rauhen Rohren. *VDI Forshungsheft* no. 361. Translated as *NACA TM*, no. 1292 (1950).

PRANDTL, L. & SCHLICHTING, H. 1934 Das Wiederstandagesetz rauher Platten. *Werft Reederei Hafen* 1–4.

ROTTA, J. C. 1950 On the theory of the turbulent boundary layer. *NACA TM*, no. 1344.

ROTTA, J. C. 1962 Turbulent boundary layers in incompressible flow. *Progr. Aero. Sci.* **2**, 5–219.

SAMS, K. W. 1952 Experimental investigations of average heat transfer and friction coefficients for air flowing in circular tubes having square-threads type roughness. *NACA Res. Mem.* RME 52017.

SCHLICHTING, H. 1937 Experimental investigation of the roughness problem. *Abridged Translation of Hydraulics Papers. Amer. Soc. Civil Engrs. Proc.* **63**, 16–31. More complete translation in *NACA TM*, no. 823.

STREETER, V. & CHU, H. 1949 Fluid flow and heat transfer in artificially roughened pipes. Final Report Project 4918, Armour Research Foundation.